Local coordination of Mn atoms at the Mn:Ge(111) interface from photoelectron diffraction experiments

A. Verdini,[1] A. Cossaro,[1] L. Floreano,[1] A. Morgante,[1,2] A. Goldoni,[3] D. Ghidoni,[4] A. Sepe,[4] S. Pagliara,[4] and L. Sangaletti[4]
[1]*Laboratorio TASC-INFM, Basovizza, 34012 Trieste, Italy*
[2]*Dipartimento di Fisica, Universitá di Trieste, via Valerio 2, 34127 Trieste, Italy*
[3]*Sincrotrone Trieste S.C.P.A., Basovizza, 34012 Trieste, Italy*
[4]*Dipartimento di Matematica e Fisica, Universitá Cattolica, via dei Musei 41, 25121 Brescia, Italy*
(Received 31 May 2007; revised manuscript received 29 November 2007; published 7 February 2008)

X-ray photoelectron diffraction (PED) experiment on the metallic Mn:Ge(111) surface alloy has been carried out in the initial stage of mixed phase growth. Our findings show that the Mn_5Ge_3 phase is not yet formed for a 1.3 ML (monolayer) coverage, as well as for a 2 ML coverage, followed by an annealing at temperature (~300 °C). Rather, we observed the formation of an ordered surface alloy by Mn occupation of the hollow H_3 sites in the topmost layer, while about 10% of Mn atoms are found in subsurface layers, partially confirming the theoretical expectations by Zhu *et al.* [Phys. Rev. Lett. **93**, 126102 (2004)]. However, the contribution to PED patterns from subsurface Mn atoms is found compatible with the occupation of interstitial sites only for the 1.3 ML coverage and with the occupation of both interstitial and unexpected substitutional sites for the 2 ML coverage. These findings thus open questions about the determination of the kinetic path to Mn subsurface migration in diluted alloys.

DOI: 10.1103/PhysRevB.77.075405 PACS number(s): 68.35.Fx, 61.05.js, 68.47.Fg

I. INTRODUCTION

The Mn:Ge(111) interface has been the subject of several studies[1–6] aimed at identifying the relationship between structural properties and ferromagnetism observed in the Mn_5Ge_3 thick layers grown onto the Ge(111) $(\sqrt{3}\times\sqrt{3})R30°$ reconstructed surface.[7] Indeed, there is evidence that this Mn:Ge(111) interface can be considered as the seed structure for growing ferromagnetic Mn_5Ge_3 epitaxial layers.[8] Recent theoretical studies on the Mn:Ge(111) interface report that Mn prevalently occupies the energetically favorable H_3 sites but it can easily diffuse into the bulk via interstitial sites, due to a slightly lower binding energy of the interstitial sites in deeper layers.[2] The corresponding hierarchy of site energies would explain the formation of thick Mn_5Ge_3 alloys by annealing (400–600 °C) of a predeposited Mn film.[7] At the moment, there is no experimental evidence of these theoretical findings. Direct space imaging techniques, such as scanning tunneling microscopy (STM), are much helpful in characterizing the topmost layer,[7] but their reliability is much lower when the effect of subsurface atoms is considered. Therefore, in order to study the Mn diffusion into the bulk, different techniques are required, such as photoelectron diffraction (PED), which is known to be extremely sensitive to the atom environment, especially for the atoms buried below the topmost layers.[10] Indeed, the photoelectrons coming from these atoms can be efficiently scattered by the atoms above them, yielding a strong signal in the intensity modulation detected by PED.

In the present study, the Mn:Ge(111) interface has been examined by PED technique in order to identify the Mn lattice sites after the deposition of a thin layer of Mn on the Ge(111) surface. We show that the for a coverage of 1.3 ML (monolayer) of Mn, the Mn atoms uniformly occupy the H_3 hollow sites in the topmost layer, in agreement with theoretical predictions by Zhu *et al.*[2] Exceeding Mn diffuses into the bulk, even at room temperature, mainly in the interstitial subsurface layers. After a mild annealing at 300 °C for a slightly larger coverage of Mn (2 ML), the occupation of both interstitial and unexpected—with respect to theoretical results—substitutional sites is found compatible with our experimental data, while about 90% of Mn atoms still uniformly occupies the H_3 hollow sites in the topmost layer. In this respect, it must be remarked that the formation of the Mn_5Ge_3 phase can be clearly excluded for the present Mn coverage and annealing treatment. As a consequence, our measurements effectively captured the initial stage of Mn subsurface migration, which should help for a better elucidation of the kinetic pathway to the growth of diluted Mn:Ge alloys.

II. EXPERIMENT

The PED measurements have been carried out at the INFM ALOISA synchrotron beamline in Trieste (Italy). The experimental setup is described in detail elsewhere.[11] The Mn $2p_{3/2}$ photoemission core line has been selected for the PED measurements with a medium kinetic energy of 305 eV (photon energy of 950 eV), in order to enhance the photoelectron yield from the Mn atoms in the bulk. The Ge(111) surface was prepared by repeated cycles of 1 keV Ar^+ ion sputtering and annealing at 700 °C, until a sharp reflection high-energy electron diffraction (RHEED) pattern was obtained, displaying the characteristic $c(2\times8)$ symmetry reconstruction of the clean surface. The deposition of Mn has been monitored by means of a quartz microbalance, which was previously calibrated by real time x-ray reflectivity measurements with several metal evaporants. The coverage has been cross-checked after growth by photoemission analysis, taking into consideration the attenuation length of photoemitted electrons. The surface structures we consider have been obtained after an evaporation of 1.3 and 2 ML thick Mn

films. For the latter, a postgrowth annealing was carried out at 300 °C for 120 s to induce the surface alloy formation. RHEED patterns have been collected along the ⟨112⟩ and ⟨110⟩ directions of the substrate. After Mn deposition, the RHEED pattern presents very weak features, which, after annealing the surface, increase in intensity and display a structural ordering identified with the $(\sqrt{3}\times\sqrt{3})R30°$ surface reconstruction (for the RHEED patterns, see Fig. 1 of Ref. 12).

The PED polar scans have been measured by collecting the photoemission signal as a function of the polar emission angle θ by rotating the electron analyzer in the scattering plane for different orientations of the surface azimuth ϕ. The incidence angle of the photon beam was kept fixed at 4.5°, with the polarization in the transverse magnetic condition and the surface normal in the scattering plane. The photoemission intensity has been measured at the maximum of the Mn $2p_{3/2}$ peak and at suitably chosen energies aside the peak, in order to allow an effective subtraction of the background due to the secondary electrons. The scanned range of the azimuth is about ±35° around the ⟨11−2⟩ symmetry direction of the substrate, and the polar scans collected around this high symmetry direction have been symmetrically folded. The experimental χ function containing the modulations (anisotropy), due to the electron diffraction, has been obtained as

$$\chi(\theta,\phi) = [I(\theta,\phi) - I_0(\theta,\phi)]/I_0(\theta,\phi), \qquad (1)$$

where $I_0(\theta,\phi)$ is the nondiffractive part of the signal obtained as a polynomial fit for each polar scan.

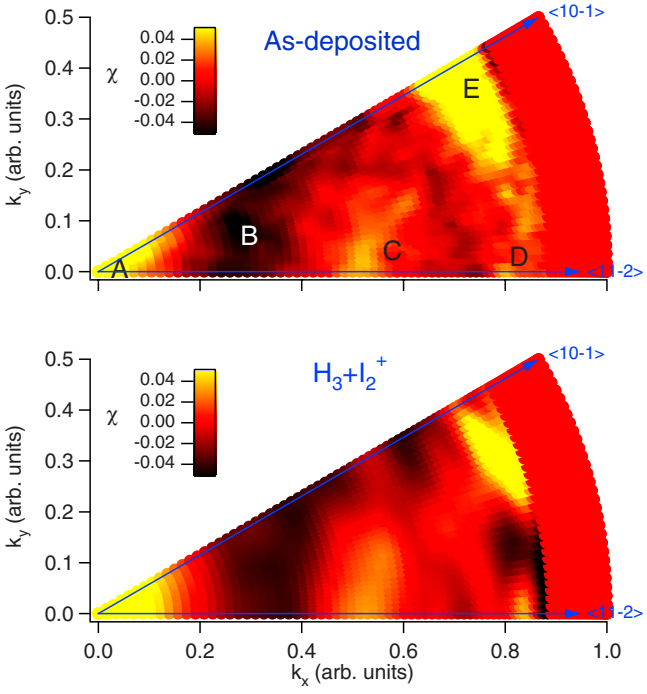

FIG. 1. (Color online) Plot of the measured anisotropy χ of the Mn $2p_{3/2}$ emission (kinetic energy of 305 eV) from the as-deposited thin film (top). The experimental polar range extends from 0° to 62° with respect to the surface normal. The simulated anisotropy for the best-fit model ($H_3+I_2^+$) is also shown for comparison (bottom).

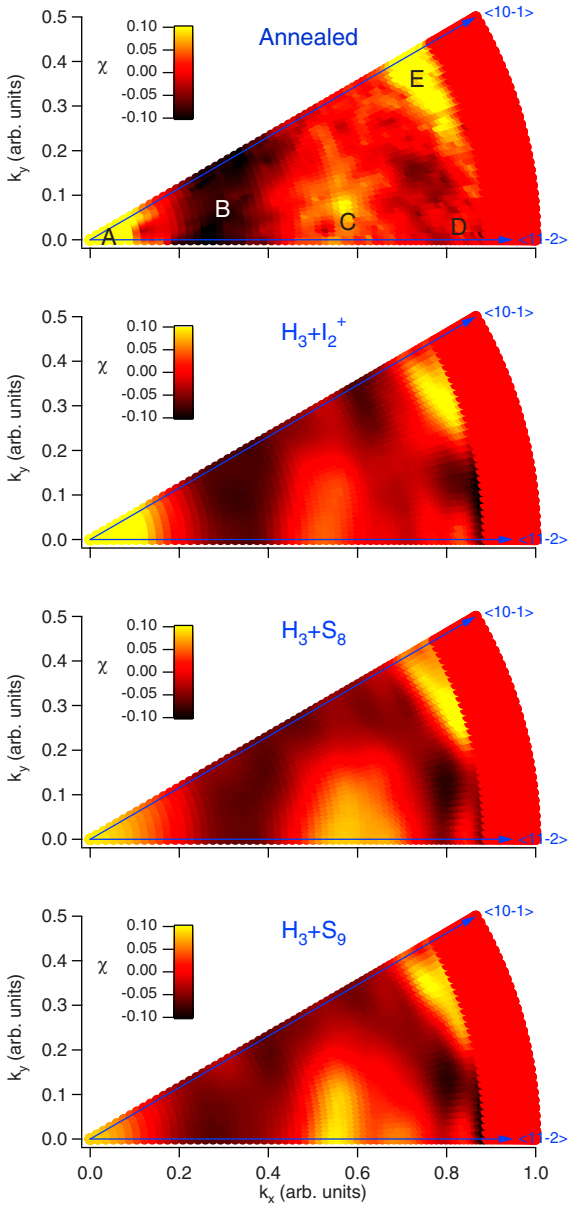

FIG. 2. (Color online) Plot of the measured anisotropy χ of the Mn $2p_{3/2}$ emission (kinetic energy of 305 eV) from the $(\sqrt{3}\times\sqrt{3})R30°$ surface of the Mn:Ge(111) system (top). The experimental polar range extends from 0° to 62° with respect to the surface normal. The simulated anisotropies for the three best-fit models, ($H_3+I_2^+$, H_3+S_8, and H_3+S_9) are also shown for comparison.

In order to identify unambiguously the crystal orientation of the Ge substrate, i.e., the ⟨11−2⟩ and ⟨−1−12⟩ directions, RHEED measurements were not helpful, since RHEED probes only the very first layers and therefore shows a sixfold symmetry where the ⟨11−2⟩ and ⟨−1−12⟩ directions are equivalent. For this reason, we resorted to identify the crystal orientation by comparing the results of site model simulations carried out both along the ⟨11−2⟩ and ⟨−1−12⟩ directions. Indeed, reliability R factors (defined below) determined for the ⟨11−2⟩ orientation resulted to better than those obtained from virtually all models referred to the ⟨−1−12⟩

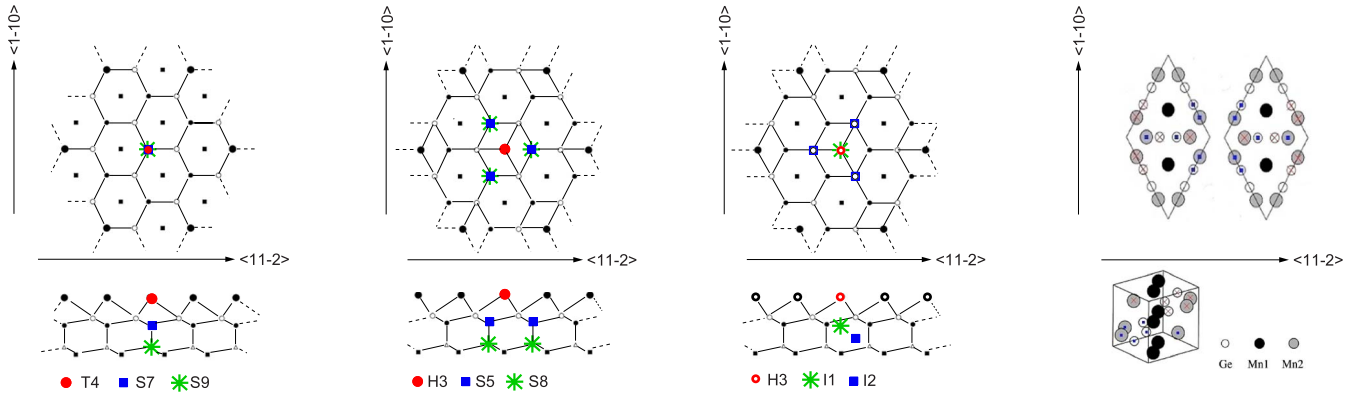

FIG. 3. (Color online) Top and side view of the interface structures around the emitting Mn atom for each model considered in the simulated PED anisotropies.

direction. Therefore, in the present study, all results will be hereafter referred to the $\langle 11-2\rangle$ orientation.

III. RESULTS AND DISCUSSION

A. X-ray photoelectron diffraction patterns

The experimental PED patterns of the as-deposited and the annealed systems are reported in Figs. 1 and 2, respectively, together with the simulations for best-fit models. A first visual examination of the Mn experimental data reveals five main features in the pattern, labeled A–E in Figs. 1 and 2: a peak along the surface normal (label A), a valley due to destructive interference (label B), a broad peak (label C) around $k_x=0.55-0.58$, and a weak peak and a long streak at low emission angles (labels D and E, respectively).

A forward scattering interpretation of the experimental data can be done by assuming that the Mn atoms occupy substitutional sites inside the bulk crystal. Apart the strong peak along the surface normal (region A), the other strong and broad peak C can be assigned to the forward scattering along the $\langle 110\rangle$ direction, while the broad peak E can be ascribed to the overlap of interference fringes due to scattering along the $\langle 110\rangle$ direction with the forward scattering along high-Miller-index directions, such as the $\langle 13-1\rangle$. These peaks are an evidence that at least a part of Mn atoms is diluted inside the crystal in substitutional sites, even when deposited at room temperature and without any annealing treatment after deposition. It should be noted that the broad peak C is about 10° large in polar and about 30° in azimuth around the $\langle 110\rangle$ direction, suggesting a possible occupation also of nonsubstitutional sites inside the crystal, maybe the interstitial ones. Moreover, if we compare the as-deposited sample PED pattern to the annealed one, it is evident that the C, D, and E features are shifted away from the surface normal. This can be due to the fact that after the annealing, the whole surface relaxes with a variation in the vertical spacing and/or some of the Mn moves toward different sites inside the crystal.

B. Comparison to the models

In order to reproduce the experimental data, several models have been simulated by placing the Mn atoms at different lattice sites on the Ge(111) topmost layers, without considering any layer adjustment (see Fig. 3). These lattice sites are the fourfold coordinated T_4 adatom site, the hollow H_3 site, the substitutional S_7, S_9, S_5, and S_8 sites, and the interstitial sites I_1 and I_2, labeled according to the schematic representation reported in Ref. 2 In addition to these models, the Mn_5Ge_3 alloy has been simulated by using the hexagonal crystal structure reported in Ref. 13 and allowing for the two possible orientations with respect to the substrate (see Fig. 3). The calculations for each model have been performed with the MSCD package,[14] with multiple scattering (MS) order up to the eighth order and a Rehr-Albers order of 2.[15] The simulated PED patterns for the possible lattice sites are shown in Fig. 4.

Unlike the analogous Pb- and Sn-Ge(111) $(\sqrt{3}\times\sqrt{3})R30°$ and (3×3) reconstructions, where Pb and Sn atoms occupy the T_4 site,[9] a visual comparison with the simulations clearly indicates that, in the present system, the contribution from the T_4 site (Fig. 4) must be discarded. Indeed, apart from a small contribution to the peak in C, the overall calculated intensity has no counterpart in the other regions (A, B, D, and E) of the experimental data. This result is consistent with former STM measurements, where no Mn atoms were found at T_4 sites already at room temperature.[7] On the other hand, the occurrence of a PED intensity maximum A along the surface normal marks a contribution that can only be originated by subsurface Mn atoms. In fact, the simulated patterns of the S_9, S_8, and I_2 sites display all of the main features A–E for both the as-deposited and the annealed systems.

For a more quantitative analysis, we adopted a modified R_a reliability factor[10,16]

$$R_a^s = min_a \frac{\sum_i (a\chi_{i,calc} - \chi_{i,expt})^2}{\sum_i [(a\chi_{i,calc})^2 + \chi_{i,expt}^2]}, \tag{2}$$

where $\chi_{i,calc}$ and $\chi_{i,expt}$ are the simulated and experimental χ values, respectively, and a is just a scaling factor which minimizes the quantity R_a^s.[17] The scaling factor, which normalizes the simulated χS, takes into account the decrease of

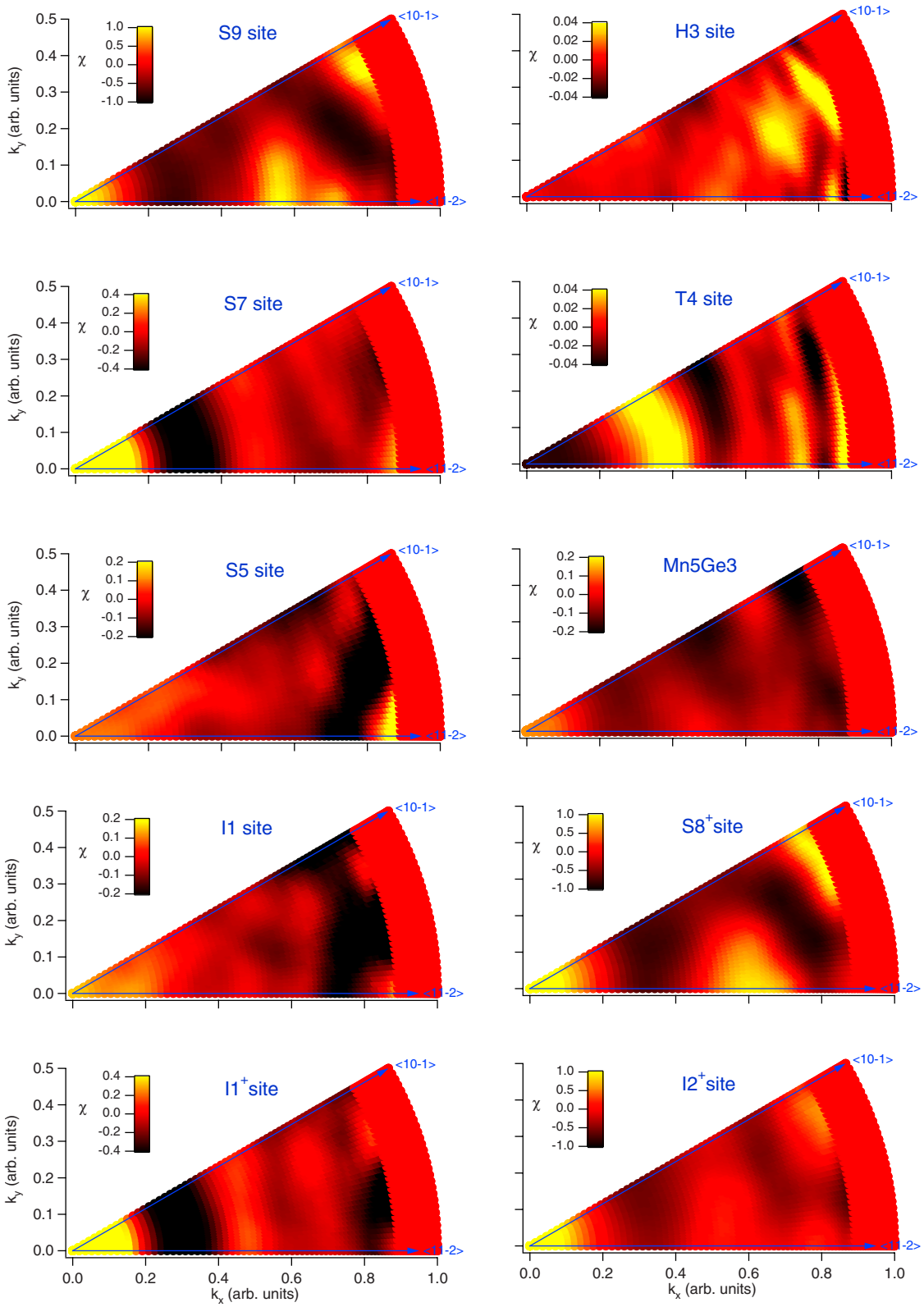

FIG. 4. (Color online) Simulated anisotropies χ for Mn atoms in different substitutional and interstitial lattice sites: the H_3 site, the T_4 site, and the Mn_5Ge_3 bulk model. For the S_8, I_1, and I_2, additional simulations (labeled S_8^+, I_1^+, and I_2^+) have been carried out, considering also a not-emitting Mn atom in H_3 site. The S_8 and I_2 simulations have been omitted, since the differences to the S_8^+ and I_2^+ are negligible. Please note the much different amplitude of the anisotropy from one site to the others. In particular, the H_3 site displays an anisotropy at least ten times lower than the substitutional sites.

TABLE I. *R*-factor comparison for the various models and the corresponding scaling factors.

	As-deposited sample		Annealed sample	
Model	Scaling factor a	R_a^s	Scaling factor a	R_a^s
I_2^+ site	0.09	0.52	0.15	0.41
S_8^+ site	0.05	0.67	0.09	0.41
S_8 site	0.05	0.68	0.09	0.42
S_9 site	0.05	0.69	0.09	0.42
I_2 site	0.09	0.66	0.16	0.49
S_7 site	0.11	0.67	0.20	0.59
I_1^+ site	0.11	0.77	0.18	0.60
H_3 site	1.00	0.72	1.00	0.82
Mn_5Ge_3	0.27	0.85	0.48	0.69
T_4 site	$\forall$	$\geqslant 1$	$\forall$	$\geqslant 1$
S_5 site	$\forall$	$\geqslant 1$	$\forall$	$\geqslant 1$
I_1 site	$\forall$	$\geqslant 1$	$\forall$	$\geqslant 1$

anisotropy in the real crystal due to defects (roughness, coverage, and disorder) surrounding the emitting atom.[18]

The results of a first comparison with the experimental data are reported in Table I where the *R*-factor values are reported, as well as the scaling factors for each simulated model. As the visual comparison points out, the best agreement for the annealed system is obtained with the S_9, S_8, and I_2 models, while H_3, S_7, and the Mn_5Ge_3 models yield larger *R* factors, and T_4, S_5, and I_1 have an *R* factor always equal or greater than one. Here, it must be stressed the large difference in the anisotropy amplitude yielded by the different models (see the inset scale in Fig. 4). In fact, the deeper the Mn emitter is, the stronger its PED contribution is, since, at the given photoelectron kinetic energy, the backward scattering, which is the only PED contribution from topmost atoms, is overwhelmed by the forward scattering from buried atoms. This means that a much larger population (1 order of magnitude) must be considered for Mn in H_3 sites to yield the same anisotropy amplitude of a Mn emitter in a third layer substitutional site (such as S_8 or S_9). The occurrence of a topmost layer with a large concentration of Mn atoms may affect the diffraction pattern from subsurface Mn emitters. As a consequence, the PED patterns for the best fitting Mn subsurface models (S_8, I_1, and I_2) have also been simulated with a not-emitting Mn atom in the H_3 site. These models are labeled as S_8^+, I_1^+, and I_2^+. The addition of a layer of Mn largely affects the (I_1 and I_2) models, while the S_8 pattern is almost unchanged. This is due to the fact that for the S_8, the Mn layer is not added, but just only substitutes the Ge one. Therefore, since the atomic numbers *Z* of Mn and Ge are 25 and 32, respectively, and the electron scattering is roughly proportional to *Z*, no large differences in the calculated patterns are expected. The overall decrease of the *R* factor, by considering the S_8^+, I_1^+, and I_2^+ models, strongly supports the hypothesis that a large part of Mn atoms is on the very surface at the hollow sites, especially for the as-deposited system where the *R* factor decreases from 0.66 to the minimum of 0.52. Since PED patterns are formed as an incoherent sum of different contributions coming from atoms emitting with different local environments, each different patterns can contribute to the overall one with a weight due to its "concentration" in the system. Therefore, we further refined our analysis by considering the superposition of the contribution to PED by Mn emitters in two different sites. If we sum up a linear combination of the single models as

$$\chi = C_1\chi_1 + C_2\chi_2, \tag{3}$$

where χ_i is the anisotropy of the *i* simulated model, it is possible to obtain an improvement of the *R* factors, as re-

TABLE II. *R*-factor comparison for the linear combination of the various models and the corresponding scaling factors. The w_i are the effective weights obtained by normalizing the sum of the scaling factors C_i to one.

Linear combination	As-deposited sample			Annealed sample		
	Scaling factors C_i	Effective weights w_i	R_a^s	Scaling factor a	Effective weights w_i	R_a^s
$H_3+Mn_5Ge_3$	1.00,0.15	0.87,0.13	0.64	1.00,0.39	0.72,0.28	0.57
$I_1^+ + H_3$	0.07,1.00	0.07,0.93	0.60	0.16,1.00	0.14,0.86	0.50
$S_7 + H_3$	0.09,1.00	0.08,0.92	0.49	0.17,1.00	0.14,0.86	0.47
$S_8 + I_2$	0.03,0.04	0.43,0.57	0.65	0.07,0.04	0.63,0.37	0.41
$S_9 + S_8$	0.02,0.03	0.40,0.60	0.67	0.04,0.05	0.44,0.56	0.41
$S_9 + I_2$	0.03,0.05	0.38,0.62	0.65	0.07,0.05	0.58,0.42	0.41
$S_9 + S_7$	0.03,0.07	0.30,0.70	0.62	0.07,0.07	0.50,0.50	0.40
$S_8 + S_7$	0.03,0.07	0.30,0.70	0.62	0.07,0.06	0.54,0.46	0.40
$I_2 + S_7$	0.04,0.06	0.40,0.60	0.65	0.07,0.06	0.54,0.46	0.40
$I_2 + H_3$	0.07,1.00	0.07,0.93	0.50	0.14,1.00	0.12,0.88	0.39
$S_9 + H_3$	0.04,1.00	0.04,0.96	0.54	0.08,1.00	0.07,0.93	0.34
$S_8 + H_3$	0.04,1.00	0.04,0.96	0.54	0.08,1.00	0.07,0.93	0.34
$I_2^+ + H_3$	0.07,1.00	0.07,0.93	0.39	0.14,1.00	0.12,0.88	0.32

ported in Table II. The $C_i=A_i w_i$ are scaling factors including both the normalization factor A_i due to "nonideal" surface structures and the relative weight w_i of the i model. The comparison with the experimental data has been done by using Eq. (2), with $a=1$ and the $\chi_{calc}=\Sigma_i C_i \chi_i$. Under the reasonable assumption that the defects that can reduce the measured anisotropy are randomly distributed ($A_i=A$), it is possible to write $C_i=A w_i$ and to estimate the effective weight $w_i=C_i/\Sigma_i C_i$ of the pattern for each single model i, as shown in Table II. It should be noted that the combination of each model structure with the H_3 model always yields an improvement of the R factor, especially for the as-deposited system where the R factor decreases from 0.52 for the I_2^+ model (Table I) to 0.39 for the $I_2^+ + H_3$ model (Table II). The three best fits to the experimental pattern of the annealed sample (R factors of 0.32 and 0.34) are obtained by combining H_3 with S_9, S_8, or I_2^+, and the resulting patterns are also shown in Fig. 2 (we did not repeated the simulation for the S_8^+ model since its pattern is virtually equivalent to the S_8 one). Our experimental data are therefore compatible with a structural model where most of the Mn atoms occupy the H_3 hollow sites in the topmost layer, and a relatively smaller population ($\sim 10\%$) is diluted in the subsurface layers, occupying substitutional (S_9 and S_8) or interstitial (I_2^+) sites. In fact, theoretical calculations indicate that the formation of a stable surface alloy by occupation of H_3 sites is favored along the Ge(111) direction.[2] Discrepancies with theoretical models are found when the occupation of subsurface sites is considered. First of all, our data are not compatible with Mn atoms in interstitial sites of type I_1, whereas this site was predicted to be energetically equivalent to the I_2 one. In particular, the I_1 was predicted to be the precursor stage to Mn subsurface migration starting from H_3 sites, since they displayed the lowest-energy barrier. In fact, our analysis sets in evidence the possible occurrence of substitutional Mn atoms in the third layer, whose total energy was predicted to be much larger than interstitial sites, and also larger than substitutional sites in the second layer, which are definitely ruled out by our analysis.

IV. CONCLUSIONS

In summary, we have been able to determine the local structural properties of the Mn:Ge(111) interface at the early stage of growth. Due to the reduced amount of Mn (1.3 and 2 ML) at the interface and to the relatively low annealing temperature (300 °C), we did not find evidence of the Mn_5Ge_3 structure. Rather, in agreement with recent calculations,[2] we observed the formation of an ordered surface alloy with Mn atoms in H_3 sites after mild annealing. The exceeding Mn atoms are diluted in the Ge bulk with a small portion that is retained in the subsurface layers (with a 1–10 relative population with respect to the surface Mn atoms). In particular, we can exclude the occurrence of Mn in the interstitial I_1 sites, and we must consider the occupation of the substitutional S_9 and S_8 sites in alternative or together with the occupation of I_2 interstitial sites. These findings are in contrast with available theoretical models[2] and ask for further theoretical investigations of the mechanisms of Mn subsurface migration in Mn:Ge diluted alloys. In addition, the overall magnetic properties of these diluted systems should be discussed by properly considering the specific contribution from the substitutional S_9, S_8, and interstitial I_2 sites.

[1] R. Gunnella, L. Morresi, N. Pinto, R. Murri, L. Ottaviano, M. Passacantando, F. D'Orazio, and F. Lucari, Surf. Sci. **577**, 22 (2005).

[2] Wenguang Zhu, H. H. Weitering, E. G. Wang, Efthimios Kaxiras, and Zhenyu Zhang, Phys. Rev. Lett. **93**, 126102 (2004).

[3] A. Stroppa, S. Picozzi, A. Continenza, and A. J. Freeman, Phys. Rev. B **68**, 155203 (2003).

[4] G. Profeta, S. Picozzi, A. Continenza, and C. Franchini, Phys. Rev. B **70**, 155307 (2004).

[5] A. Continenza, F. Antoniella, and S. Picozzi, Phys. Rev. B **70**, 035310 (2004).

[6] J. Kudrnovsky, I. Turek, V. Drchal, F. Maca, P. Weinberger, and P. Bruno, Phys. Rev. B **69**, 115208 (2004).

[7] Changgan Zeng, Wenguang Zhu, Steven C. Erwin, Zhenyu Zhang, and Hanno H. Weitering, Phys. Rev. B **70**, 205340 (2004).

[8] Changgan Zeng, S. C. Erwin, A. P. Li, R. Jin, Y. Song, J. R. Thompson, and H. H. Weitering, Appl. Phys. Lett. **83**, 5002 (2003).

[9] J. J. Metois and G. Le Lay, Surf. Sci. **133**, 422 (1983); J. S. Pedersen, R. Feidenhans'l, M. Nielsen, K. Kjaer, F. Grey, and R. L. Johnson, *ibid.* **189/190**, 1047 (1987); G. Le Lay, K. Hricovini, and J. E. Bonnet, Appl. Surf. Sci. **41/42**, 25 (1989); L. Floreano, L. Petaccia, M. Benes, D. Cvetko, A. Goldoni, R. Gotter, L. Grill, A. Morgante, A. Verdini, and S. Modesti, Surf. Rev. Lett. **6**, 1091 (1999); L. Petaccia, L. Floreano, M. Benes, D. Cvetko, A. Goldoni, L. Grill, A. Morgante, A. Verdini, and S. Modesti, Phys. Rev. B **63**, 115406 (2001).

[10] D. P. Woodruff and A. M. Bradshaw, Rep. Prog. Phys. **57** 1029 (1994); C. S. Fadley, in *The Study of Surface Structures by Photoelectron Diffraction and Auger Electron Diffraction*, edited by R. Z. Bachrach, Synchrotron Radiation Research: Advances in Surface and Interface Science Vol. 1 (Plenum, New York, 1992).

[11] L. Floreano, G. Naletto, D. Cvetko, R. Gotter, M. Malvezzi, L. Marassi, A. Morgante, A. Santaniello, A. Verdini, F. Tommasini, and G. Tondello, Rev. Sci. Instrum. **70**, 3855 (1999); R. Gotter, A. Ruocco, A. Morgante, D. Cvetko, L. Floreano, F. Tommasini, and G. Stefani, Nucl. Instrum. Methods Phys. Res. A **467-468**, 1468 (2001).

[12] L. Sangaletti, D. Ghidoni, S. Pagliara, A. Goldoni, A. Morgante, L. Floreano, A. Cossaro, M. C. Mozzati, and C. B. Azzoni, Phys. Rev. B **72**, 035434 (2005).

[13] J. B. Forsyth and P. J. Brown, J. Phys.: Condens. Matter **2**, 2713 (1990).

[14] Y. Chen, F. J. Garcia de Abajo, A. Chasse', R. X. Ynzunza, A. P. Kaduwela, M. A. Van Hove, and C. S. Fadley, Phys. Rev. B **58**,

13121 (1998); for updated information, see http://www.sitp.lbl.gov/

[15] The convergence of the simulations has been checked by comparing the simulated patterns obtained by increasing the MS order and the number of atoms. The phase shifts needed have been obtained using muffin-tin potentials for the Mn and Ge atoms calculated with the MUFPOT codes of Pendry (Ref. 16), whose radii have been chosen to be 1.25 Å for Mn and 1.15 Å for Ge (about 90% of the bond length for their stable bulk structure).

[16] J. B. Pendry, *Low Energy Electron Diffraction* (Academic, London, 1974).

[17] A. Verdini, M. Sambi, F. Bruno, D. Cvetko, M. Della Negra, R. Gotter, L. Floreano, A. Morgante, G. A. Rizzi, and G. Granozzi, Surf. Rev. Lett. **6**, 1201 (1999).

[18] R. S. Saiki, A. P. Kaduwela, M. Sagurton, J. Osterwalder, D. J. Friedman, C. S. Fadley, and C. R. Brundle, Surf. Sci. **33-61**, 282 (1993).